HIPPOCAMPUS 15:950–962 (2005)

Theta Oscillation-Coupled Dendritic Spiking Integrates Inputs on a Long Time Scale

Zsófia Huhn,[1] Gergő Orbán,[1,2] Péter Érdi,[1,3] and Máté Lengyel[4*]

ABSTRACT: Persistent neural activity lasting for seconds after transient stimulation has been observed in several brain areas. This activity has been taken to be indicative of the integration of inputs on long time scales. Passive membrane properties render neural time constants to be on the order of milliseconds. Intense synaptic bombardment, characteristic of in vivo states, was previously shown to further reduce the time scale of effective integration. We explored how long-term integration in single cells could be supported by dendritic spikes coupled with the theta oscillation, a prominent brain rhythm often observed during working memory tasks. We used a two-compartmental conductance-based model of a hippocampal pyramidal cell to study the interplay of intrinsic dynamics with periodic inputs in the theta frequency band. We show that periodic dendritic spiking integrates inputs by shifting the phase relative to an external oscillation, since spiking frequency is quasi-linearly modulated by current injection. The time-constant of this integration process is practically infinite for input intensities above a threshold (the integration threshold) and can be still several hundred milliseconds long below the integration threshold. The somatic compartment received theta frequency stimulation in antiphase with the dendritic oscillation. Consequently, dendritic spikes could only elicit somatic action potentials when they were sufficiently phase-shifted and thus coincided with somatic depolarization. Somatic depolarization modulated the frequency but not the phase of firing, endowing the cell with the capability to code for two different variables at the same time. Inputs to the dendrite shifted the phase of dendritic spiking, while somatic input was modulating its firing rate. This mechanism resulted in firing patterns that closely matched experimental data from hippocampal place cells of freely behaving rats. We discuss the plausibility of our proposed mechanism and its potential to account for the firing pattern of cells outside the hippocampus during working memory tasks. © 2005 Wiley-Liss, Inc.

KEY WORDS: active dendrites; persistent activity; working memory; place cells; phase precession

INTRODUCTION

Pyramidal cells in the cerebral cortex have extended dendritic arbors integrating inputs from thousands of presynaptic cells (Hausser et al., 2000). Active voltage-dependent conductances play a central role in shaping this integration process: they can boost distal inputs so that their effect on somatic firing becomes level with that of proximal inputs (Cook and Johnston, 1997), make the summation of postsynaptic potentials (PSPs) sub- or supralinear, defying the predictions of standard cable theory (Rall, 1959, 1989), and hence endow single neurons with computational powers identical to those of a network of point-neurons (Poirazi et al., 2003). In some cases, sufficiently strong stimulation is able to elicit dendritic spikes (Spencer and Kandel, 1961; Wong et al., 1979), which thus represent an extreme case of these nonlinear processing capabilities. Such dendritic regenerative potentials are considered to be the final outcomes of local dendritic integration, which ultimately influence somatic action potential generation (Golding and Spruston, 1998) or local synaptic plasticity (Golding et al., 2002).

Most of the studies of nonlinear dendritic processing focused on the spatial aspects of integration, while its temporal aspects have attracted relatively little attention. In this paradigm, PSPs are integrated in a potentially complicated way to produce a change in dendritic membrane potential depending on their amplitudes, slopes, and dendritic locations, but the membrane potential at any time depends only on the immediate past of the neuron's input (Reyes, 2001). Crucially, the window of temporal integration is assumed to be small, as it is determined by the time constants of the PSPs and the membrane time constant, none of which exceeds usually tens of milliseconds (Rall, 1989; Destexhe et al., 1998).

Active conductances in some cases seem to further reduce the effective time constant of dendrites. Although dendritic cable filtering may smear out distally evoked PSPs by the time they reach the soma so that they summate on a longer time scale (Rall, 1959), a voltage-dependent current, the hyperpolarization-activated I_h current, was shown to counteract this and produce location-independent PSP time-courses in the soma (Magee, 1999). This seems to be at odds with findings showing that many neuron types, including cortical pyramidal cells, are able to integrate inputs on long time scales. The most striking example of this is when transient inputs lead to persistent changes in neural firing rates that last for several hundred milliseconds or even seconds (Major and Tank, 2004).

Another often neglected factor is the effect that ongoing in vivo population activity has on the way a neuron integrates its inputs. Intense bombardment of

[1]**Biophysics Department, KFKI Research Institute for Particle and Nuclear Physics, Hungarian Academy of Sciences, Budapest, Hungary;** [2]**Collegium Budapest, Institute for Advanced Study, Budapest, Hungary;** [3]**Center for Complex Systems Studies, Kalamazoo College, Kalamazoo, Michigan;** [4]**Gatsby Computational Neuroscience Unit, University College London, London, UK**

Grant sponsor: Gatsby Charitable Foundation; Grant sponsor: Hungarian Scientific Research Fund (OTKA); Grant number: T038140; Grant sponsor: Henry R. Luce Foundation.

*Correspondence to: Máté Lengyel. E-mail: lmate@gatsby.ucl.ac.uk

Accepted for publication 15 June 2005
DOI 10.1002/hipo.20112
Published online 17 August 2005 in Wiley InterScience (www.interscience.wiley.com).

the dendritic tree with synaptic inputs is the characteristic of in vivo states (Destexhe et al., 2003), and this was shown to decrease the membrane resistance (Williams, 2004). As a consequence, it should also decrease the membrane time constant (Bernander et al., 1991), thereby, further reducing the effective time scale of dendritic integration. In accordance with this, morphologically and electrophysiologically realistic computational modeling showed that neurons can process their inputs with a high temporal resolution under these conditions (Rudolph and Destexhe, 2003a). However, previous studies used constant (Williams, 2004) or stationary (Bernander et al., 1991; Rudolph and Destexhe, 2003a,b) background activity as a model of in vivo network activity, while cortical networks are known to exhibit behavior-dependent oscillations on several time scales (Buzsáki and Draguhn, 2004). In particular, blocking theta oscillation in rodents was shown to cause impairment in both spatial and nonspatial working memory tasks, for which persistent activity seems to be crucial (Winson, 1978; Givens and Olton, 1990; Mizumori et al., 1990). Moreover, human and nonhuman primate experiments have shown that execution of working memory tasks is often accompanied by cortical theta oscillations (Gevins et al., 1997; Tesche and Karhu, 2000; Kahana et al., 2001; Jensen and Tesche, 2002).

Persistent neuronal activity has been extensively studied and was implicated as the neural basis of working memory (Fuster, 2001). Although proposed network mechanisms for generating persistent activity proliferate (Seung, 1996; Koulakov et al., 2002; Goldman et al., 2003; Machens et al., 2005), long-term integration has also been observed in in vitro entorhinal cortex preparations in which synaptic transmission was blocked, suggesting potent single-cell mechanisms (Egorov et al., 2002). Graded persistent activity in this case is generated by self-sustaining plateau potentials, which, in turn, were shown to depend on a muscarinic-activated calcium-sensitive nonspecific cation current (Andrade, 1991; Klink and Alonso, 1997; Fransen et al., 2002). While this mechanism allows for multistability of firing rates, it does not account for firing rates changing within trials (ramping up, down, etc; reviewed in Major and Tank, 2004), nor it is clear how robust this mechanism is in the face of massive in vivo-like, potentially oscillating synaptic activity. Moreover, induction of plateau potentials usually requires long (over 500 μs) stimulation. Depolarizing after potentials have also been suggested to underlie persistent network acitivy during working memory tasks, also taking into account the possible effects of theta oscillations (Jensen et al., 1996), but this class of models still predicts strictly constant within-trial firing rates.

Here, we use a simplified biophysical model neuron to investigate how periodic dendritic spiking contributes to the integration of inputs on long time scales during one of the most prominent brain rhythms, the hippocampal theta oscillation (Vanderwolf, 1969; Buzsáki, 2002). In vivo population activity was shown to facilitate the compartmentalization of dendrites, so that they integrate their inputs independently of somatic events (Williams, 2004), and also to promote the generation and propagation of dendritic spikes (Destexhe and Pare, 1999; Williams, 2004). Regular dendritic spiking was observed in the hippocampus during theta oscillations (Kamondi et al., 1998; Gillies et al., 2002), and the frequency of dendritic oscillations could be modulated by the amount of current injected (Kamondi et al., 1998). We propose that under these conditions, periodic dendritic spiking integrates inputs in its spiking phase relative to the ongoing field potential oscillation, and the decay time constant of this integration can be several orders of magnitude longer than the membrane time constant.

The somatic membrane potential of hippocampal pyramidal cells is periodically modulated during theta oscillations (Leung and Yim, 1986; Fox, 1989; Soltész and Deschenes, 1993; Ylinen et al., 1995), and the ability of dendritic spikes evoking somatic action potentials was shown to depend on the level of somatic depolarization (Golding and Spruston, 1998; Williams, 2004). We show that this provides a potential mechanism for transforming the phase code of dendritic spikes into a firing rate code, as the number of somatic action potentials fired within a theta cycle depends on the phase of the dendritic spike relative to the somatic membrane potential oscillation. The phase of somatic action potentials also reflects the phase of the dendritic spike, but it can be decoupled from the rate code by changing levels of somatic depolarization, so that the firing phase and rate of a cell code for different variables, just as seen in recent experiments in behaving animals (Huxter et al., 2003). We test further predictions of our model on the firing patterns of hippocampal pyramidal cells by comparing them with data recorded from place cells in rats.

METHODS

We used a modified Pinsky–Rinzel (Pinsky and Rinzel, 1994) two-compartmental conductance-based model of a hippocampal CA3 pyramidal cell. Active conductances were the fast Na^+ current, the delayed rectifier K^+ current in the somatic, the noninactivating Ca^{2+} current, and the Ca^{2+}-dependent K^+ current in the dendritic compartment. For detailed description of the equations and model parameters see the Appendix.

Dendritic input was the sum of two terms: $I_d(t) = I_{d\theta}(t) + I_{dv}(t)$. $I_{d\theta}$ was a sinusoid depolarizing current: $I_{d\theta}(t) = (A_d/2)\cos(2\pi f_\theta t) + I_{d0}$, where $f_\theta = 8$ Hz, and other parameters were $A_d = 0.5$ μA/cm^2 and $I_{d0} = 1.615$ μA/cm^2 (Figs. 1 and 2) or 1.9 μA/cm^2 (Fig. 3) or 1.78 μA/cm^2 (Figs. 4 and 5), unless otherwise noted. I_{dv} was a current proportional to the variable that was to be integrated by dendritic dynamics. This variable was $\upsilon(t)$, the running speed of the rat within the place field of the cell in Figures 4 and 5: $I_{dv}(t) = k_d\upsilon(t)$, where $k_d = 0.024$ (μA/cm^2)/(cm/s).

Somatic input was also a sum of two terms: $I_s(t) = I_{s\theta}(t) + I_{sv}(t)$. $I_{s\theta}$ was a sinusoid current oscillating with theta frequency in antiphase with the dendritic sinusoid input: $I_{s\theta}(t) = (A_s/2)\cos(2\pi f_\theta t + \pi) + I_{s0}$, where $A_s = 5$ μA/cm^2, and $I_{s0} = -3.5$ μA/cm^2 (Fig. 3) or $I_{s0} = -4.9$ μA/cm^2 (Figs. 4 and 5), unless otherwise noted. I_{sv} was a current proportional to the variable to be encoded in somatic firing rate. This variable was again

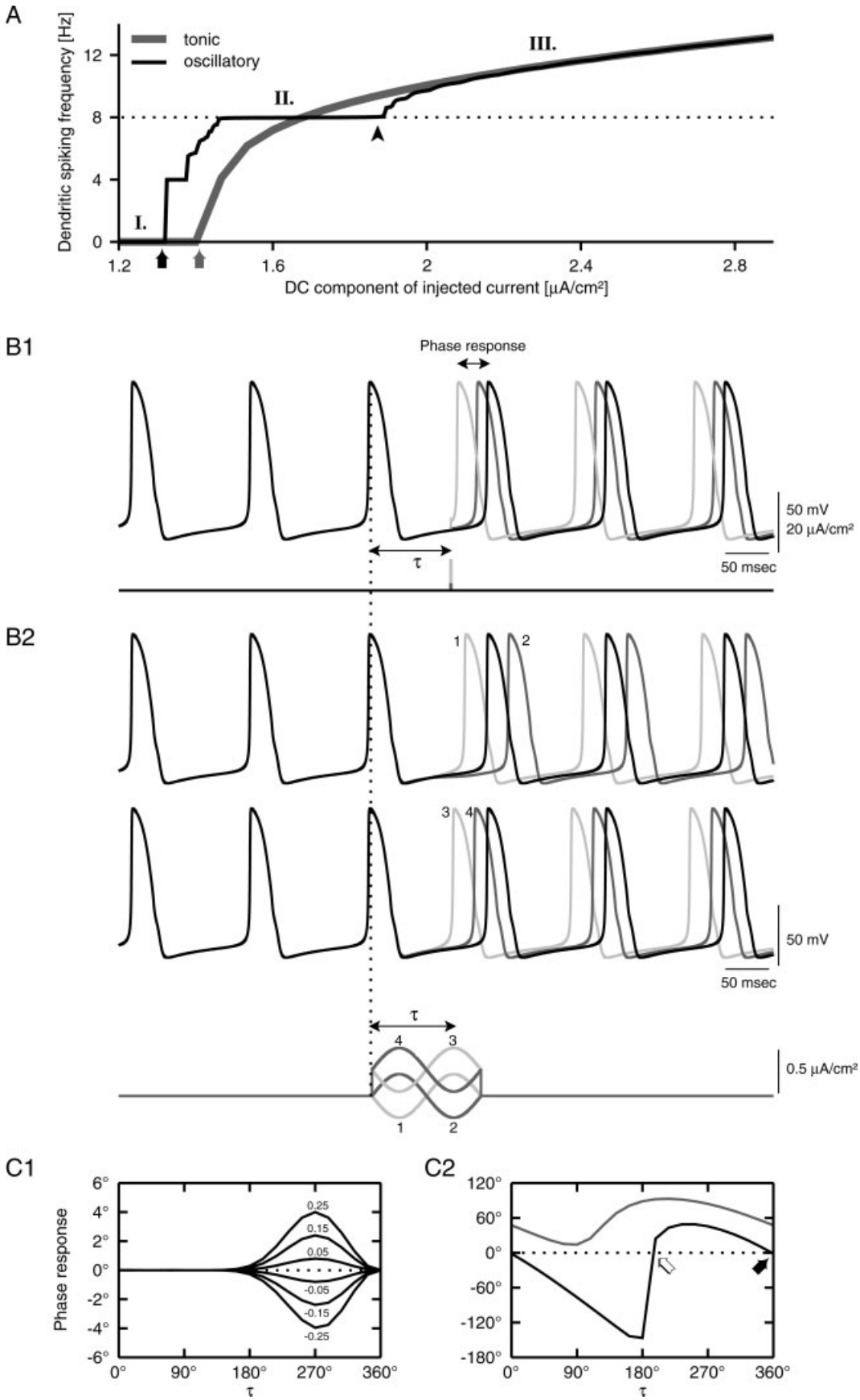
A
tonic
oscillatory
I.
II.
III.
Dendritic spiking frequency [Hz]
DC component of injected current [μA/cm²]
B1
Phase response
τ
50 mV
20 μA/cm²
50 msec
B2
1
2
3
4
50 mV
50 msec
0.5 μA/cm²
C1
Phase response
0.25
0.15
0.05
-0.05
-0.15
-0.25
τ
C2
τ

FIGURE 1

the running speed of the rat within the place field of the cell in Figures 4 and 5: $I_{sv}(t) = k_a \upsilon(t)$, where $k_s = 0.1$ ($\mu A/cm^2$)/(cm/s).

For Figures 4 and 5, a total of 50 traversals of the place field were simulated. In each lap, a random running speed profile was generated by choosing a different speed between 10 and 30 cm/s for the rat, with a uniform distribution after every 100 ms. To ensure that the rat could enter the place field at any phase of theta, the time of the first speed change was randomly chosen from the 0 to 100 ms interval, with a uniform distribution. Finally, speed profiles were smoothed with a Gaussian kernel of 100 ms standard deviation, and position was calculated as the time integral of the respective speed profile. In Figure 5, "fast" and "slow" runs were chosen to be the fastest and slowest 15 runs based on average running speed within the place field. Moving direction of the animal was always from left to right (Figs. 4 and 5).

RESULTS

Dendritic Spiking

We used a biophysical conductance-based model composed of a dendritic and a somatic compartment to investigate the integration of inputs in pyramidal cells. The dendritic compartment contained active currents that enabled it to generate slow Ca^{2+} spikes in response to sufficiently strong depolarization (Fig. 1A, gray line). The frequency–current (f–I) curve of the dendrite showing the frequency of dendritic spiking as a function of the amplitude of tonic depolarization exhibited clear Type-1 behavior (Ermentrout, 1996): as depolarization exceeded the threshold for spike generation, spiking frequency increased monotonically from 0 Hz.

Superimposing a small oscillatory component on the tonic depolarizing current (the DC component) changed the f–I relationship substantially (Fig. 1A, black line), resulting in three qualitatively different regimes of dendritic dynamics. Below spiking threshold no dendritic spikes were generated (regime I). The spiking threshold was decreased and above it the f–I curve quickly became flat over a range of depolarization strengths (regime II). In this regime, dendritic spiking frequency was determined by the frequency of the oscillatory component of external stimulation and was independent of the DC component. As further depolarization exceeded a second threshold, the integration threshold, it led to increasing spiking frequency, which was primarily determined by the DC component of external stimulation, as the f–I curve quickly became overlapping with the curve recorded in response to nonoscillatory stimulation (regime III).

Importantly, in regime III, the frequency of dendritic spiking was higher than the frequency of the oscillatory component of the stimulus. When two oscillations have different frequencies, they cannot be phase locked anymore, and the amount of phase shift between them will be proportional both to their frequency difference and to the length of time for which their frequencies differed. In other words, frequency modulated oscillations integrate inputs in their phase: as long as the frequency is an approximate linear function of the input, the phase of the oscillation will be the time integral of the input (Lengyel et al., 2003). To demonstrate this, we injected a strong depolarizing current into the dendrite that elicited periodic dendritic spiking at about 8 Hz (Fig. 1B). A short perturbing pulse current on top of this depolarization caused a phase shift in the dendritic

FIGURE 1. Characteristics of periodic dendritic spiking induced by constant and oscillatory stimulation. A: Spiking frequency of the dendritic compartment as a function of the DC component of injected current (f–I curve). Above firing threshold (gray arrow), tonic stimulation (thick gray line) resulted in increasing spiking frequencies. Oscillatory stimulation (thin black line) resulted in a decreased spiking threshold (black arrow, regime I) and frequency locking to the oscillatory input (dotted line) in a wide range of the DC component (regime II). Above integration threshold (black arrowhead, see text), the frequency of dendritic firing quickly converged to the tonic depolarization induced f–I curve (regime III). B: Phase responses of the dendritic oscillation to transient stimulation. B1: Illustration of the stimulation protocol. Constant stimulation (lower black line) caused periodic spiking in the dendrite of the pyramidal cell model (upper black trace). A 1 ms pulse current superimposed on the constant depolarization (lower gray lines) induced a shift in dendritic spiking (upper gray traces). This phase response depended on the timing of the pulse relative to the spiking cycle (τ), as well as its amplitude (light and dark gray membrane potential traces). Note that both the phase response and τ are measured in degrees relative to the dendritic interspike interval (ISI). B2: Phase responses of the dendrite resulting from periodic stimulation. A single cycle of sinusoid current with a given offset and phase superimposed on the tonic stimulation (lower panel) caused either both delay and advance of dendritic spiking (upper panel) or only advance (middle panel), depending on stimulus offset. Upper and middle panel: black traces are dendritic membrane potentials with tonic stimulation, gray traces correspond to dendritic membrane potentials resulting from transient periodic stimulation. Labels and colors correspond to those used in the lower panel. Note that here τ denotes the time of the peak of the oscillatory component relative to the ongoing dendritic oscillation. C: Phase response curves of the dendritic compartment as a result of current pulse stimulation (C1) and oscillatory stimulation (C2). Positive phase response means advance (shorter ISI) and negative means delay (longer ISI). C1: Current pulse stimulation with positive pulse-amplitudes (positive labels) resulted in strictly positive phase response curves. Phase response curves scaled linearly with pulse amplitude (labels denote pulse amplitudes in $\mu A/cm^2$). C2: Oscillatory phase response curves (oPRCs), calculated with the protocol illustrated in B2, at different offset currents (0 and 0.3 $\mu A/cm^2$ for the black and gray lines, respectively). While at low offset-levels, both positive and negative phase shifts could be achieved, causing advanced or delayed spiking (black line), and at high offset levels only positive phase shifts were available (gray line). At zero-crossing a stable (black arrow) and an unstable fixed point (white arrow) are present depending on the slope of the oPRC. At high offset-levels, no fixed points are present, causing a continuous shift in the phase of spiking. Note that the black curve corresponds to regime II while the gray curve corresponds to regime III of the f–I curve (A).

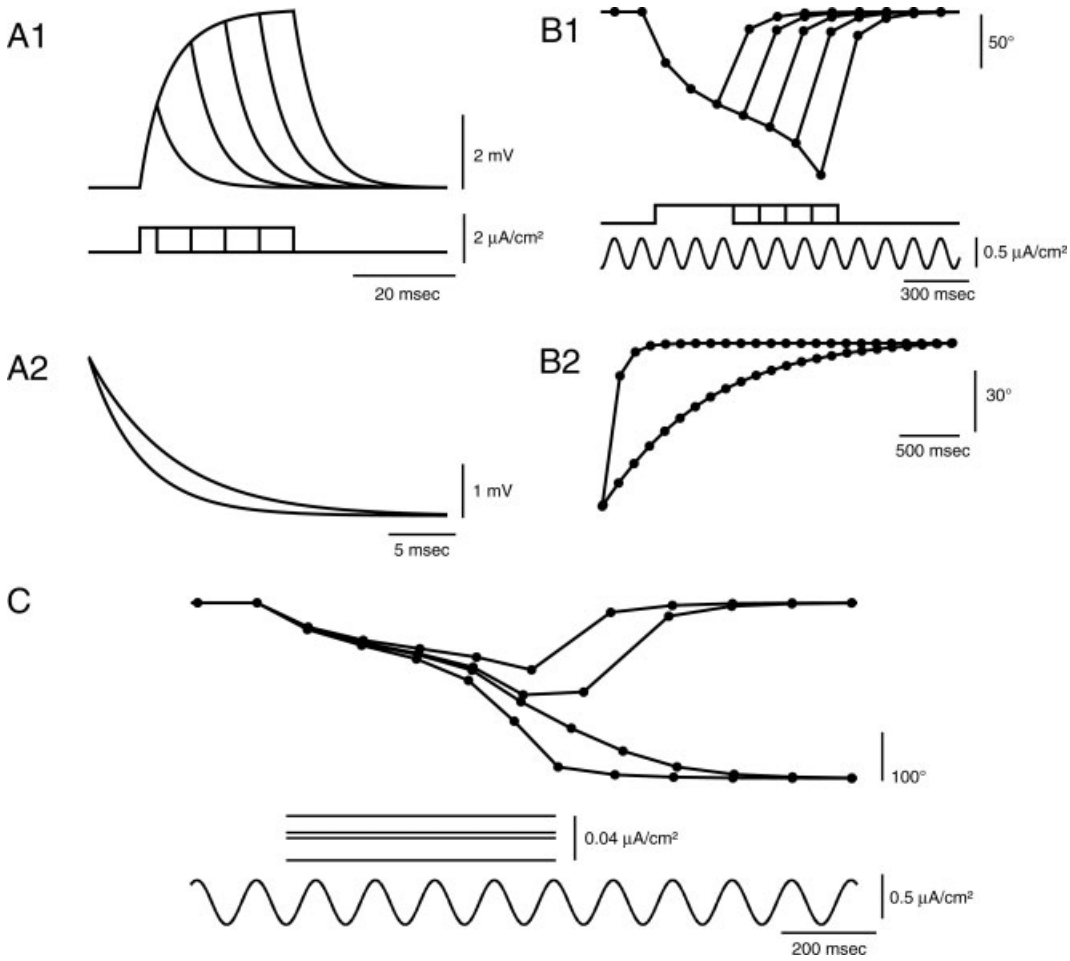

FIGURE 2. Comparison of input integration in dendritic membrane potential and in the phase of dendritic spiking. Note the difference between the scale bars in A and B, indicating the difference of the integration time scale in the two cases. A: Below spiking threshold, current pulses of increasing length (A1, lower traces) induced saturating membrane potential change (A1, upper traces). Time scale of the integration process was determined by the membrane time constant (A2, 4 and 2.86 μs for the upper and lower trace, respectively). B: Above integration threshold, current pulses (B1, middle traces) induced the advancement of dendritic spiking (upper traces) relative to the periodic stimulation (lower trace). Total amount of phase precession increased monotonously and without saturation as the length of stimulation was increased. Phase of dendritic firing settled to the stable phase after stimulation returned to baseline level (regime II). Time course of decay dynamics of dendritic spiking-phase (B2) was determined by the amplitude of the oscillatory component (0.5 and 0.05 μA/cm^2 for the upper and lower trace, respectively). C: After cessation of stimulation, phase of dendritic spiking relative to the periodic stimulation component settled to the stable phase either by advancing spiking phase (upper panel, lower two traces) or by delaying it (upper panel, upper two traces). Whether phase precession or phase recession occurred depended on the spiking phase at the end of regime III stimulation. Here, different exit phases were achieved by slight changes in the DC components (middle panel, duration of the simulation corresponds to the extent of the lines, and DC levels correspond to respective traces of the upper panel in a reversed order).

oscillation (Fig. 1B1). The amount of the phase shift depended on the phase of the dendritic oscillation at which the perturbing current was delivered: perturbation was effective only in the second half of the spiking cycle (Fig. 1C1). Moreover, the size of the phase shift was linear in the amplitude of the perturbing current, within a range of pulse amplitudes (Fig. 1C1).

To analyze the effect of an oscillatory current injection, a full cycle of sine wave stimulus was applied on top of the baseline stimulus, with different starting phases and offset values (Fig. 1B2). Oscillatory inputs with small offsets could both advance or delay the next dendritic spike, depending on the starting phase of the stimulation (Fig. 1B2, upper trace). Spiking was advanced when the dendritic spike lagged behind the peak of the sine wave stimulus and delayed when the dendritic spike occurred before the peak of the sine wave stimulus (Fig. 1C2, black line). This means that applying the same oscillatory current for several cycles drives dendritic spiking so that it becomes phase-locked to this external oscillation. As long as the oscillatory phaseresponse curve (oPRC) crosses zero with a negative slope there is a stable phase lag for dendritic spiking (a crossing with positive slope indicates an unstable phase lag), and thus, its frequency is kept at the frequency of the external

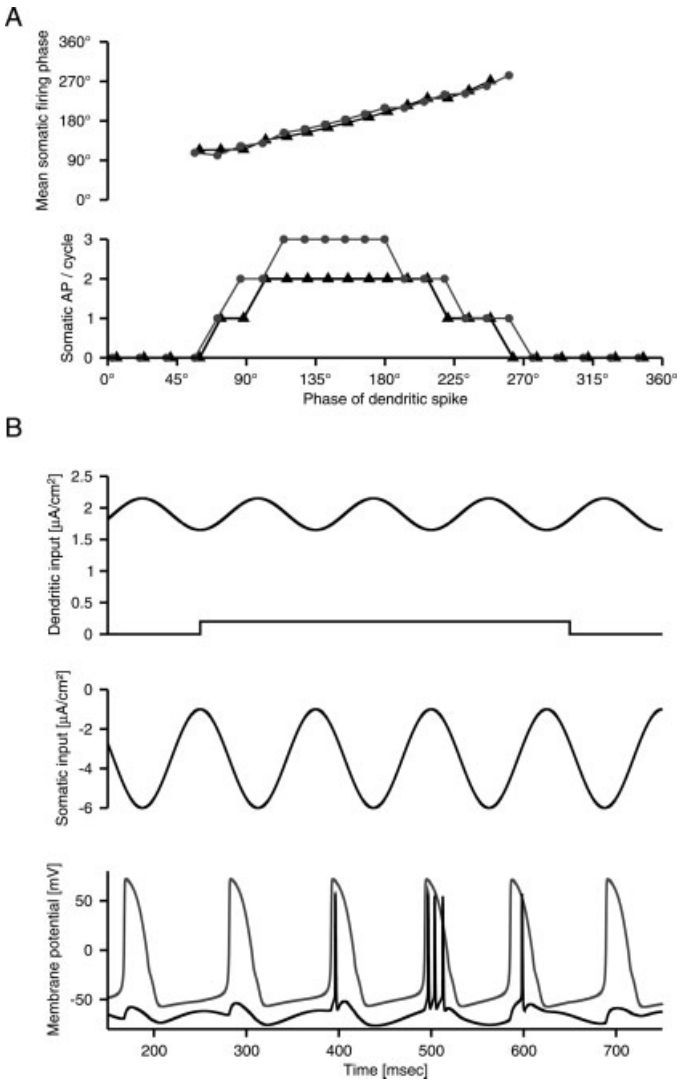

FIGURE 3. Somatic read-out of dendritic integration. A: DC component of somatic stimulation did not affect the mean phase of somatic action potentials (upper panel), but had a significant effect on the number of somatic action potentials fired per oscillation cycle (lower panel): increased DC components resulted in higher number of action potentials per cycle. DC components were −3.5 and −4 μA/cm^2 for the gray and black symbols, respectively. Zero degree corresponds to the phase of strongest somatic hyperpolarization here and hereafter. B: Phase precession of action potentials. Hyperpolarizing subthreshold oscillatory input delivered to the soma (middle panel) was set antiphase with the oscillatory component of the dendritic stimulation (upper panel, upper trace). When DC dendritic input (upper panel, middle trace) was below integration threshold, dendritic spiking was phase-locked to the oscillatory component of dendritic input. As a result of the antiphasic relationship, dendritic spiking could not elicit somatic action potentials (first 300 μs in the plot). Pushing the dendrite over the integration threshold by a small current pulse, dendritic spiking precessed, thus, the overlap between dendritic spiking and somatic oscillatory increased. At the same time, number of somatic action potentials increased up to the maximum overlap and decreased again as the dendritic spikes were generated earlier than the maximum of the somatic input.

stimulation (regime II of the f–I curve, Fig. 1A). Oscillatory current injection with an elevated offset could only cause spike advance (Fig. 1B2, lower trace), shifting the oPRC above zero at all phase lags (Fig. 1C2, gray line), as it amounted to an overall excitation above the integration threshold (regime III of the f–I curve, Fig. 1A).

We compared the integrative properties of two dynamical modes of the dendritic membrane. Without strong baseline depolarization, the dendrite integrated inputs in its membrane potential (Fig. 2A) as determined by its passive properties (Rall, 1959). Long time scale integration in this mode was hampered in two ways. First, the membrane potential became quickly saturated for long inputs, instead of increasing linearly with stimulus length. Second, after the cessation of the stimulus the membrane potential returned to its resting value within tens of milliseconds (Fig. 2A1), instead of staying constant. The rate of this decay and, therefore, the time constant of integration was determined by the membrane time constant (Fig. 2A2).

Strong oscillatory baseline stimulation (regime II) elicited periodic dendritic spiking, and the phase precession of dendritic spiking was roughly proportional to the length of dendritic stimulation above the integration threshold (Fig. 2B1). The slight curvature in the phase shift curve was attributable to the sinusoid shape of the oPRC (Fig. 1C2, gray line): its distance from the zero axis was uneven, and therefore, phase shifts were bigger or smaller when dendritic spiking lagged or led the peak of the external oscillation, respectively. In the absence of extra stimulation, the oscillatory component of baseline stimulation drove dendritic spiking back to the stable phase lag shown in Figure 1C2 in a few theta cyles. However, the speed of this decay could be slowed down dramatically by decreasing the amplitude of the oscillatory component to the input (Fig. 2B2). As spiking phase is a circular variable, decay back to baseline phase could occur in one of two ways. It occurred either through phase precession or through phase recession, depending on what the spiking phase was at the end of stimulation (Fig. 2C), just as predicted by the oPRC of the dendritic membrane (Fig. 1C2). In summary, in the periodically spiking regime, the dendrite integrated inputs above the integration threshold near-perfectly, and behaved as a leaky integrator with a time constant much longer than its membrane time constant for inputs below this threshold.

Somatic Firing

The somatic compartment of the model cell contained currents for firing fast Na^+ action potentials. In response to a subthreshold theta-frequency current injection, its membrane potential went through periodic cycles of depolarization and hyperpolarization. This provided a straightforward read-out mechanism for the phase code of dendritic spiking (Fig. 3).

If the dendrite spiked in the hyperpolarized phase of the soma, the dendritic spike could not invade and no somatic action potentials were fired. However, the more the dendritic spike overlapped with somatic depolarization, the more action

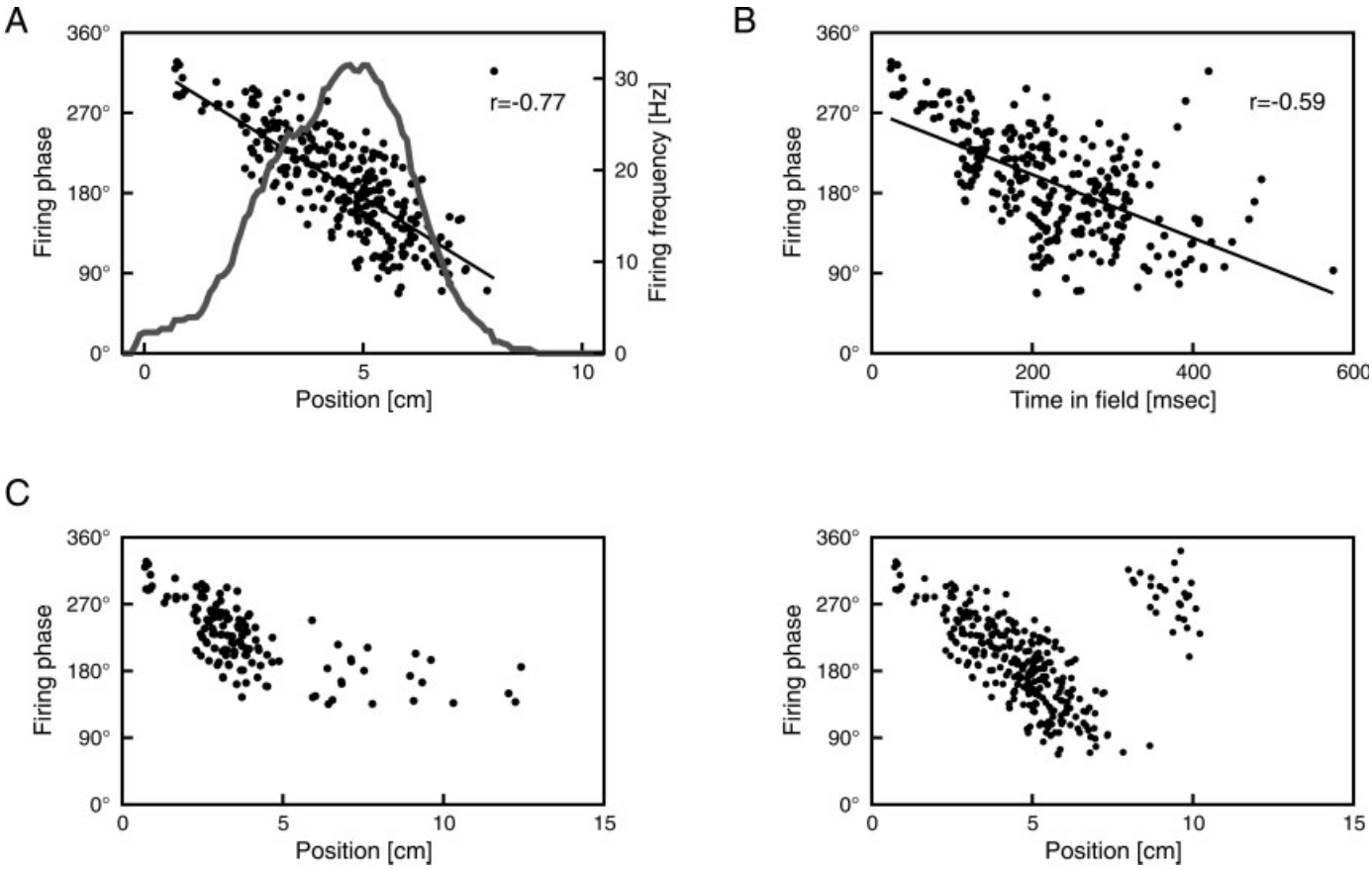

FIGURE 4. Rate and phase coding in place cells as reproduced by the model. A: While phase of somatic firing (black dots) is a monotonically decreasing function of position, the firing rate has a unimodal profile (gray line). Comparison of firing phase data plotted against position (A) and that plotted against the time spent in the place field (B) reveals a higher correlation (*r*) with position than with time. Black lines are regression lines fitted on data points. Aggregate data from multiple traversals of the place field is presented, where speed of the animal was subject to change both during a single traversal and across traversals. C: Phase precession did not require precise tuning of place field size: whether the phase precession was less than a full cycle of theta oscillation (left panel) or was longer than a cycle (right panel), the place cell ceased to fire action potentials shortly after leaving the place field.

potentials the soma could fire. This resulted in doubly coded somatic firing (Lengyel et al., 2003): dendritic spiking phase was reflected in both the phase of somatic spikes and the number of spikes during a theta cycle (Fig. 3A).

The DC component of somatic input could decouple the phase and rate code of somatic firing (Fig. 3A, gray lines). Firing phase was largely unaffected by increasing DC somatic input, as it was still determined by the timing of dendritic spikes, while firing rate increased because depolarization of the somatic membrane between consecutive action potentials was accelerated. This decoupling has not been demonstrated in previous models (Lengyel et al., 2003).

As the sinusoid components of dendritic and somatic inputs were set to be in antiphase and dendritic spikes were phase-locked to the dendritic oscillation at baseline (Figs. 1C2 and 2B1), somatic firing rate was low without extra excitation (Fig. 3B). When the input current exceeded the integration threshold, dendritic spikes began to phase shift, thus, becoming increasingly in-phase with somatic depolarization and resulting in an increasing number of somatic action potentials. As phase precession of dendritic spiking continued because of sustained input, dendritic spikes became out-of-phase with somatic depolarization and somatic firing rate decreased accordingly. This periodic waxing and waning of somatic firing rate could continue as long as dendritic input was present (data not shown).

Comparison with Place Cell Data

Pyramidal cells of the hippocampus are known to exhibit location-specific firing in the behaving rat: a "place cell" only fires when the rat is in a circumscribed region of the environment, the "place field" of the cell (O'Keefe and Dostrovsky, 1971). Place cell recordings thus provide detailed quantitative in vivo data on the firing patterns of hippocampal pyramidal cells, against which we tested the predictions of our model.

As suggested by earlier modeling (Lengyel et al., 2003; Lengyel and Érdi, 2004), we took dendritic input to be proportional to the running speed of the animal. Because position is the time-integral of velocity, the phase of dendritic spiking

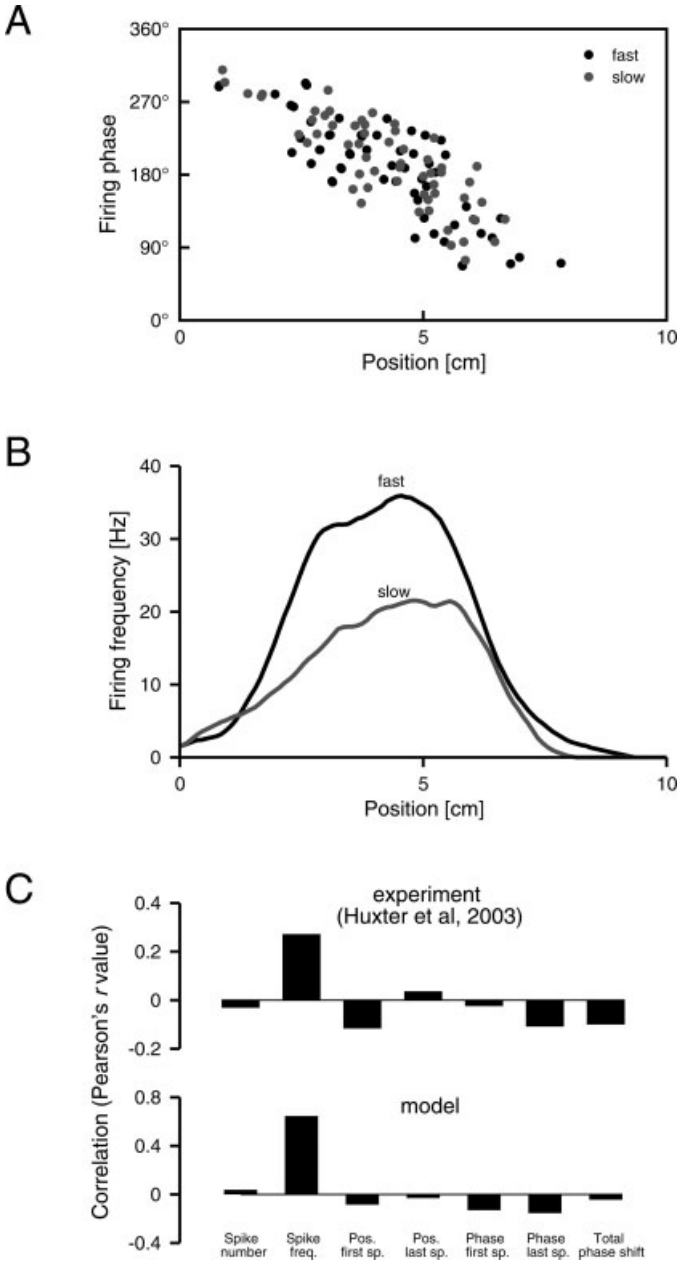

FIGURE 5. Decoupling the rate and phase code. Firing phase data collected from fast (A, black) and slow (gray) place field traversals had an overlapping profile. Firing rate tuning curves (B), however, were significantly different, faster runs peaking at higher levels than slower runs. C: Analysis of the running speed-dependence of the rate and phase code. Correlation coefficients between running speed and various characteristics of place cell firing were calculated (lower panel). Labels denote number of spikes fired in the place field (spike number), average firing frequency (spike freq.), position of the animal in the place field when the first (pos. first sp.) and last (pos. last sp.) spike was fired, phase of the first (phase first sp.) and last (phase last sp.) spike relative to theta oscillation, and the total phase shift in the place field. The most significant correlation was measured between running speed and average firing frequency. Data obtained from simulations and experiments (upper panel, Huxter et al., 2003) were closely matching.

became proportional with the position of the animal as it kept integrating running speed. The somatic read-out mechanism (Fig. 3) thus ensured that both firing rate and firing phase of somatic action potentials coded for the position of the animal. In line with earlier modeling studies using abstract models (Lengyel et al., 2003), this produced a unimodal firing rate tuning curve and a monotonically decreasing phase precession curve spanning a full cycle of theta oscillation (Fig. 4A), where firing phase was more correlated with position than with time spent in the place field (Fig. 4B), just as seen in experiments (O'Keefe and Recce, 1993; Huxter et al., 2003). Our simulations did not seem to show the occasionally observed scalopped shape of phase precession data (Skaggs et al., 1996, but see O'Keefe and Recce, 1993; Huxter et al., 2003).

However, overall phase shift of place cells always amounts to an integer number of theta cycles (usually just a single theta cycle) (O'Keefe and Recce, 1993; Skaggs et al., 1996). This may not seem to be reproduced by our model unless the integral of dendritic input is exactly matched, so that dendritic spiking is ensured to precess an integer number of theta cycles. Furthermore, if phase precession does not stop after spanning a full cycle of theta oscillation, the model predicts sustained firing after the animal leaves the place field of the cell. Contrary to these inauspicious expectations, the model stopped firing even when the integral of dendritic input was not exactly matched to produce one cycle of dendritic phase precession (Fig. 4C). This happened because after the cessation of input, free-running phase shift drove dendritic spiking back to the stable baseline firing phase at which it was phase-locked to the dendritic oscillation (Figs. 1C2 and 2C) and therefore could not evoke somatic firing (Fig. 3). Such an inertia-like behavior of place cell firing was observed in experiments when rats were made to turn around before reaching the end of a place field (Redish et al., 2000). As changes in firing phase are determined by the internal dynamics of the dendrite during free-running phase shift, this mechanism also predicts a smaller correlation between firing phase and position of the animal in the second half of the place field than in the first half. A decline in correlations between firing phase and position within the place field was also demonstrated in experiments (Mehta et al., 2002; Yamaguchi et al., 2002).

Our two-compartmental model also predicted that the DC component of the somatic input should modulate the firing rate of the cell while leaving firing phases relatively unaffected (Fig. 3A). If this somatic input is proportional to the running speed of the animal, then this results in a specific decoupling of the rate and phase code of place cells (Fig. 5). Faster runs through the same place field should be associated with higher firing rates while the firing phase–position relationship should not show any systematic changes (Fig. 5A and B). Indeed, such a decoupling of firing phase and rate has been found in place cells (Huxter et al., 2003), and the relative magnitude of correlation coefficients found in experiments were well-matched by the predictions of our model (Fig. 5C). Thus, the two-compartmental mechanism proposed here was capable of encoding (the integral of) one variable in the firing phase of the neuron while modulating its firing rate depending on a second variable.

DISCUSSION

Plausibility of Periodic Dendritic Spiking

Dendritic spikes are traditionally considered to be the final outcomes of dendritic integration: they signal that net local input to the dendrite exceeds a given threshold (the spike generation threshold) (Williams and Stuart, 2003). We propose that periodic dendritic spikes convey information by the change in their timing rather than by their appearance per se. A similar scenario has been suggested earlier (Marder et al., 1996) for somatic firing, but because periodic firing is a prerequisite for this type of coding, constant firing rates had to be assumed. This does not seem to be consistent with the firing pattern of cortical pyramidal cells undergoing substantial firing rate modulations (Major and Tank, 2004). In our model, although the dendrite regularly generates spikes, somatic action potentials are only triggered when a dendritic spike coincides with somatic depolarization, thereby resulting in systematically varying somatic firing rates (Figs. 3, 4).

The mechanism for dendritic spike generation in our model is admittedly simplified: it is an interplay of a low-threshold noninactivating Ca^{2+} current, and a Ca^{2+}- and voltage-dependent K^{+} current (Pinsky and Rinzel, 1994). Pyramidal cell dendrites possess a much richer repertoire of voltage-gated channels, and therefore exhibit more complex dynamics than that demonstrated here (Magee et al., 1998; Hausser et al., 2000; Reyes, 2001). Nevertheless, we expect the main findings of our work to apply as long as dendrites are shown to be able to behave as Type I oscillators (Fig. 1). Periodic Ca^{2+} spikes in pyramidal cell dendrites during hippocampal theta oscillations were observed in vitro (Gillies et al., 2002) and in vivo (Kamondi et al., 1998), and the frequency of dendritic oscillations could be modulated by the amount of depolarization (Kamondi et al., 1998), in line with the predictions of the model (Fig. 1). However, whether these suprathreshold oscillations are of Type I remains to be tested, as there have yet been no systematic studies on the f–I curves or PRCs of pyramidal cell dendrites.

The amplitude of experimentally observable dendritic spikes also tends to be smaller (around 10 mV, Kamondi et al., 1998; Gillies et al., 2002) than that of the full-blown Ca^{2+} spikes seen in the model (Fig. 1B, 3B). This is important because these spikes may then not be able to propagate to the soma and ever elicit somatic action potentials, thus undermining a crucial assumption of our model. Yet, in other studies, dendritic spikes were shown to actively propagate towards the soma and trigger fast action potentials there in vitro (Golding and Spruston, 1998) and under emulated in vivo-like conditions (Williams, 2004). It is not clear what causes this discrepancy in experimental findings. One possibility is that the amplitude of dendritic spikes appeared smaller in some experiments (Kamondi et al., 1998; Gillies et al., 2002) because they were not recorded at the site of their generation. This also raises an interesting issue about how multiple potential spike-generating compartments may interact in the same dendritic tree, or how dendritic morphology may influence the propagation of dendritic spikes (Vetter et al., 2001). Models with more detailed morphology than the extremely simplified two-compartmental structure used here will be needed for studying such interactions.

Firing Patterns Indicative of Theta Oscillation-Coupled Long-Time Scale Integration in Behaving Animals

Current experimental techniques do not yet permit routine dendritic recordings in freely behaving animals, although they may soon become available (Helmchen et al., 2001). We used data from place cell recordings to test whether the neural firing patterns seen in exploring rats are consistent with our proposed dendritic integration mechanism (Fig. 4, 5). We found that even fine details of place cell firing were accounted for by the model, such as relative correlations between firing phase and position (Fig. 4A and C) or time spent in the place field (Fig. 4B) (O'Keefe and Recce, 1993; Huxter et al., 2003), and correlations between running speed and various quantitative characteristics of firing (Fig. 5) (Huxter et al., 2003). Results on phase precession at low firing rates ($\sim$1 spike per second) are controversial (Harris et al., 2002; Huxter et al., 2003). Although we did not address this issue in our simulations explicitly, the structure of the model predicts phase precession even at minimal frequencies.

Our modeling of place cell data is also consistent with several earlier proposals that the hippocampus and surrounding areas may be involved in path integration (McNaughton et al., 1996; Redish and Touretzky, 1997; Samsonovich and McNaughton, 1997; Sharp, 1997). However, a recent study by Zugaro et al. (2005) showed that hippocampal cells continued phase precessing after transient intrahippocampal perturbation that otherwise seemed to disrupt hippocampal theta activity. This renders the interpretation of simple integration models like the one presented here (O'Keefe and Recce, 1993; Lengyel et al., 2003) less straightforward, and points to alternative or, at least, additional mechanisms for explaining place cell firing (Burgess et al., 1994; Jensen and Lisman, 1996; Tsodyks et al., 1996; Wallenstein and Hasselmo, 1997; Mehta et al., 2002; Yamaguchi, 2003). These models assume that an area outside the hippocampus keeps track of the current position of the animal and thus may still be consistent with the experiments of Zugaro et al. (2005) in which the entorhinal cortex was shown to be unaffected by the perturbation. In our model, the integration process takes place in the distal dendrite of hippocampal pyramidal cells that receives perforant path input from the entorhinal cortex. Thus, if the dynamics of Ca^{2+} spike generation are resistant enough to comissural (proximal) perturbation, our mechanism might still be able to account for the Zugaro et al. (2005) data. Calcium dynamics underlying plateau potentials have been shown to be robust to prolonged hyperpolariza-

tions (Fransen et al., 2002); further studies are needed to investigate the robustness of calcium spiking mechanisms.

Persistent activity of putative pyramidal cells in the hippocampus was also observed during the delay period of a delayed nonmatch-to-sample task (Deadwyler and Hampson, 2004). Although field potentials were not recorded in these experiments, other studies had found hippocampal theta activity while animals performed tasks similar to these (Givens and Olton, 1990; Givens, 1996). Hence, our model predicts that if the ramping activity seen in these cells is really generated within the hippocampus and not transmitted from upstream areas, these cells should also show gradual phase precession during the delay period.

In a recent study, Lee et al. (2005) recorded neurons in monkey extrastriate visual cortex during a working memory task. They also found a significant enhancement of theta oscillations during the delay period, where theta power was shown to be directly related to the memory component of the task and not to other nonspecific effects. Several neurons showed elevated firing rates during the same period, and most importantly, their firing rate and phase strongly covaried (cf. our Fig. 3A). Moreover, the preferred phase of firing was very similar across neurons. These data are highly consistent with the behavior of our model.

The Role of Theta Oscillations

Three aspects of theta oscillations are essential for the integration mechanism of our model. (1) The dendritic membrane has to be depolarized sufficiently over the spike generation threshold, so that dendritic spikes can integrate inputs in their timing (Fig. 1). In line with this, the dendritic membrane of hippocampal pyramidal cells was found to be depolarized during theta oscillations and spontaneously generates spikes with theta frequency (Kamondi et al., 1998, and see above). (2) Depolarization of the dendritic membrane needs to have a periodic component with theta frequency, so that there is a threshold (the integration threshold, Fig. 1) under which noisy inputs do not influence dendritic integration. The oscillatory dendritic input also serves as a reference signal against which the timing of dendritic spikes can be "measured." Pyramidal cell dendrites also showed subthreshold theta frequency oscillations and dendritic spikes rode on the peaks of these oscillations (Kamondi et al., 1998), just as predicted by the model under baseline conditions (Figs. 1C2, 2B and C, and 3B). (3) The somatic membrane needs to be periodically hyperpolarized with the same frequency, so that somatic action potentials are fired depending on the relative phase of dendritic spikes. The somatic and dendritic oscillations have to be in antiphase, so that the cell fires minimally under baseline conditions (Fig. 3). Hyperpolarizing somatic membrane potential oscillations have been described in pyramidal cells during theta oscillation, and these oscillations were in antiphase with the dendritic oscillation (Kamondi et al., 1998; Gillies et al., 2002).

Thus it seems that all conditions are provided for our model to perform long time scale integration—at least in the hippocampus. In particular, the activity of different subclasses of interneurons, specifically innervating different regions of the denritic trees of pyramidal cells (Freund and Buzsáki, 1996), as well as the input from the entorhinal cortex are strongly theta modulated (Csicsvári et al., 1999; Frank et al., 2001; Klausberger et al., 2003) and their preferred firing phases support the specific theta-related effects required by our theory. Yet, integration on long time scales was observed in several brain areas (Major and Tank, 2004) and was suggested to serve a number of purposes from stabilizing eye position (Seung, 1996) to integrating evidence for decision making (Gold and Shadlen, 2002). Whether theta oscillations satisfy the above conditions in brain regions other than the hippocampus remains to be tested.

It is, nevertheless, suggestive that short-term memory tasks are often accompanied by theta oscillations (Kahana et al., 2001; Jensen and Lisman, 2005), and the presence of theta oscillations was shown to be necessary for successful performance in these tasks (Winson, 1978; Givens and Olton, 1990; Mizumori et al., 1990; Pan and McNaughton, 1997). Other models have been proposed to account for this (Lisman and Idiart, 1995; Jensen and Lisman, 1998), but they predict relatively constant firing rates within trials, while our model accommodates time-varying firing rates, such as the ramping behavior often seen in these experiments (Baeg et al., 2003; Brody et al., 2003; Deadwyler and Hampson, 2004). Modulatory effects of theta oscillations on synaptic plasticity are suggested to account for reversal learning in the model of Hasselmo et al. (2002). These authors did not address the issue of working memory, explicitly, and the memory trace necessary for performing reversal correctly in the simulated task was encoded in synaptic weights rather than persistent activity. It would be interesting to see how similar modulatory effects could be incorporated into our model framework.

As the sensitivity of the dendritic membrane to inputs in our model depends on the phase at which the input arrives (Fig. 1C), the timing of inputs has a profound effect on the efficacy of dendritic integration. This may also offer some insight into why different brain areas show synchronization and an increase in coherency in the theta band during short-term memory tasks (Macrides et al., 1982; Sarnthein et al., 1998; Stam et al., 2002; Fell et al., 2003; Seidenbecher et al., 2003; Mizuhara et al., 2004; Sauseng et al., 2004).

Acknowledgments

We thank Peter Latham for useful discussions, and John Huxter for kindly providing experimental data on place field statistics (Fig. 5C).

REFERENCES

Andrade R. 1991. Cell excitation enhances muscarinic cholinergic responses in rat association cortex. Brain Res 548:81–93.

Baeg EH, Kim YB, Huh K, Mook-Jung I, Kim HT, Jung MW. 2003. Dynamics of population code for working memory in the prefrontal cortex. Neuron 40:177–188.

Bernander O, Douglas RJ, Martin KA, Koch C. 1991. Synaptic background activity influences spatiotemporal integration in single pyramidal cells. Proc Natl Acad Sci USA 88:11569–11573.

Brody CD, Hernandez A, Zainos A, Romo R. 2003. Timing and neural encoding of somatosensory parametric working memory in macaque prefrontal cortex. Cereb Cortex 13:1196–1207.

Burgess N, Recce M, O'Keefe J. 1994. A model of hippocampal function. Neural Netw 7:1065–1081.

Buzsáki G. 2002. Theta oscillations in the hippocampus. Neuron 33:325–340.

Buzsáki G, Draguhn A. 2004. Neuronal oscillations in cortical networks. Science 304:1926–1929.

Cook EP, Johnston D. 1997. Active dendrites reduce location dependent variability of synaptic input trains. J Neurophysiol 78:2116–2128.

Csicsvári J, Hirase H, Czurkó A, Mamiya A, Buzsáki G. 1999. Oscillatory coupling of hippocampal pyramidal cells and interneurons in the behaving rat. J Neurosci 19:274–287.

Deadwyler SA, Hampson RE. 2004. Differential but complementary mnemonic functions of the hippocampus and subiculum. Neuron 42:465–476.

Destexhe A, Pare D. 1999. Impact of network activity on the integrative properties of neocortical pyramidal neurons in vivo. J Neurophysiol 81:1531–1547.

Destexhe A, Mainen ZF, Sejnowski TJ. 1998. Kinetic models of synaptic transmission. In: Koch C, Segev I, editors. Methods in neuronal modeling. 2nd ed. Cambridge, MA: MIT Press/A Bradford Book. p 251–291.

Destexhe A, Rudolph M, Paré D. 2003. The high-conductance state of neocortical neurons in vivo. Nat Rev Neurosci 4:739–751.

Egorov AV, Hamam BN, Fransen E, Hasselmo ME, Alonso AA. 2002. Graded persistent activity in entorhinal cortex neurons. Nature 420:173–178.

Ermentrout B. 1996. Type I membranes, phase resetting curves, and synchrony. Neural Comput 8:979–1001.

Fell J, Klaver P, Elfadil H, Schaller C, Elger CE, Fernandez G. 2003. Rhinalhippocampal theta coherence during declarative memory formation: interaction with gamma synchronization? Eur J Neurosci 17:1082–1088.

Fox SE. 1989. Membrane potential and impedance changes in hippocampal pyramidal cells during theta rhythm. Exp Brain Res 77:283–294.

Frank LM, Brown EN, Wilson MA. 2001. A comparison of the firing properties of putative excitatory and inhibitory neurons from CA1 and the entorhinal cortex. J Neurophysiol 86:2029–2040.

Fransen E, Alonso AA, Hasselmo ME. 2002. Simulations of the role of muscarinic-activated calcium-sensitive nonspecific cation current INCM in entorhinal neuronal activity during delayed matching tasks. J Neurosci 22:1081–1097.

Freund TF, Buzsáki G. 1996. Interneurons of the hippocampus. Hippocampus 6:347–470.

Fuster JM. 2001. The prefrontal cortex-an update: time is of the essence. Neuron 30:319–333.

Gevins A, Smith ME, McEvoy L, Yu D. 1997. High-resolution EEG mapping of cortical activation related to working memory: effects of task difficulty, type of processing, and practice. Cereb Cortex 7:374–385.

Gillies MJ, Traub RD, LeBeau FE, Davies CH, Gloveli T, Buhl EH, Whittington MA. 2002. A model of atropine-resistant theta oscillations in rat hippocampal area CA1. J Physiol 543:779–793.

Givens BS. 1996. Stimulus-evoked resetting of the dentate theta rhythm: relation to working memory. Neuroreport 8:159–163.

Givens BS, Olton DS. 1990. Cholinergic and GABAergic modulation of medial septal area: effect on working memory. Behav Neurosci 104:849–855.

Gold JI, Shadlen MN. 2002. Banburismus and the brain: decoding the relationship between sensory stimuli, decisions, and rewards. Neuron 36:299–308.

Golding NL, Spruston N. 1998. Dendritic sodium spikes are variable triggers of axonal action potentials in hippocampal CA1 pyramidal neurons. Neuron 21:1189–1200.

Golding NL, Staff NP, Spruston N. 2002. Dendritic spikes as a mechanism for cooperative long-term potentiation. Nature 418:326–331.

Goldman MS, Levine JH, Major G, Tank DW, Seung HS. 2003. Robust persistent neural activity in a model integrator with multiple hysteretic dendrites per neuron. Cereb Cortex 13:1185–1195.

Harris KD, Henze DA, Hirase H, Leinekugel X, Dragoi G, Czurkó A, Buzsáki G. 2002. Spike train dynamics predicts theta-related phase precession in hippocampal pyramidal cells. Nature 417:738–741.

Hasselmo ME, Bodelon C, Wyble BP. 2002. A proposed function for hippocampal theta rhythm: separate phases of encoding and retrieval enhance reversal of prior learning. Neural Comput 14:793–817.

Hausser M, Spruston N, Stuart GJ. 2000. Diversity and dynamics of dendritic signaling. Science 290:739–744.

Helmchen F, Fee MS, Tank DW, Denk W. 2001. A miniature head-mounted two photon microscope. High-resolution brain imaging in freely moving animals. Neuron 31:903–912.

Huxter J, Burgess N, O'Keefe J. 2003. Independent rate and temporal coding in hippocampal pyramidal cells. Nature 425:828–832.

Jensen O, Lisman JE. 1996. Hippocampal CA3 region predicts memory sequences: accounting for the phase precession of place cells. Learn Mem 3:279–287.

Jensen O, Lisman JE. 1998. An oscillatory short-term memory buffer model can account for data on the Sternberg task. J Neurosci 18:10688–10699.

Jensen O, Lisman JE. 2005. Hippocampal sequence-encoding driven by a cortical multiitem working memory buffer. Trends Neurosci 28:67–72.

Jensen O, Tesche CD. 2002. Frontal theta activity in humans increases with memory load in a working memory task. Eur J Neurosci 15:1395–1399.

Jensen O, Idiart M, Lisman JE. 1996. Physiologically realistic formation of autoassociative memory in networks with theta/gamma oscillations: role of fast NMDA channels. Learn Mem 3:243–256.

Kahana MJ, Seelig D, Madsen JR. 2001. Theta returns. Curr Opin Neurobiol 11:739–744.

Kamondi A, Acsády L, Wang XJ, Buzsáki G. 1998. Theta oscillation in somata and dendrites of hippocampal pyramidal cells in vivo: activity-dependent phase precession of action potentials. Hippocampus 8:244–261.

Klausberger T, Magill PJ, Márton LF, Roberts JD, Cobden PM, Buzsáki G, Somogyi P. 2003. Brain-state- and cell-type-specific firing of hippocampal interneurons *in vivo*. Nature 421:844–848.

Klink R, Alonso AA. 1997. Ionic mechanisms of muscarinic depolarization in entorhinal cortex layer II neurons. J Neurophysiol 77:1829–1843.

Koulakov AA, Raghavachari S, Kepecs A, Lisman JE. 2002. Model for a robust neural integrator. Nat Neurosci 5:775–782.

Lee H, Simpson GV, Logothetis NK, Rainer G. 2005. Phase locking of single neuron activity to theta oscillations during working memory in monkey extrastriate visual cortex. Neuron 45:147–156.

Lengyel M, Érdi P. 2004. Theta modulated feed-forward network generates rate and phase coded firing in the entorhino-hippocampal system. IEEE Trans Neural Netw 15:1092–1099.

Lengyel M, Szatmáry Z, Érdi P. 2003. Dynamically detuned oscillations account for the coupled rate and temporal code of place cell firing. Hippocampus 13:700–714.

Leung LS, Yim CY. 1986. Intracellular records of theta rhythm in hippocampal CA1 cells of the rat. Brain Res 367:323–327.

Lisman JE, Idiart MAP. 1995. Storage of 7 ± 2 short-term memories in oscillatory subcycles. Science 267:1512–1515.

Machens CK, Romo R, Brody CD. 2005. Flexible control of mutual inhibition: a neural model of two-interval discrimination. Science 307:1121–1124.
Macrides F, Eichenbaum HB, Forbes WB. 1982. Temporal relationship between sniffing and the limbic theta rhythm during odor discrimination reversal learning. J Neurosci 2:1705–1717.
Magee J, Hoffman D, Colbert C, Johnston D. 1998. Electrical and calcium signaling in dendrites of hippocampal pyramidal neurons. Annu Rev Physiol 60:327–346.
Magee JC. 1999. Dendritic I_h normalizes temporal summation in hippocampal CA1 neurons. Nat Neurosci 2:508–514.
Major G, Tank D. 2004. Persistent neural activity: prevalence and mechanisms. Curr Opin Neurobiol 14:675–684.
Marder E, Abbott LF, Turrigiano GG, Liu Z, Golowasch J. 1996. Memory from the dynamics of intrinsic membrane currents. Proc Natl Acad Sci USA 93:13481–13486.
McNaughton BL, Barnes CA, Gerrard JL, Gothard K, Jung MW, Knierim JJ, Kudrimoti H, Qin Y, Skaggs WE, Suster M, Weaver KL. 1996. Deciphering the hippocampal polyglott: the hippocampus as a path integration system. J Exp Biol 199:173–185.
Mehta MR, Lee AK, Wilson MA. 2002. Role of experience and oscillations in transforming a rate code into a temporal code. Nature 417:741–746.
Mizuhara H, Wang LQ, Kobayashi K, Yamaguchi Y. 2004. A long-range cortical network emerging with theta oscillation in a mental task. Neuroreport 15:1233–1238.
Mizumori SJ, Perez GM, Alvado MC, Barnes CA, McNaughton BL. 1990. Reversible inactivation of the medial septum differentially affects two forms of learning in rats. Brain Res 528:12–20.
O'Keefe J, Dostrovsky J. 1971. The hippocampus as a spatial map. Preliminary evidence from unit activity in the freely moving rat. Brain Res 34:171–175.
O'Keefe J, Recce ML. 1993. Phase relationship between hippocampal place units and the EEG theta rhythm. Hippocampus 3:317–330.
Pan WX, McNaughton N. 1997. The medial supramammillary nucleus, spatial learning and the frequency of hippocampal theta activity. Brain Res 764:101–108.
Pinsky PF, Rinzel J. 1994. Intrinsic and network rythmogenesis in a reduced Traub model for CA3 neurons. J Comput Neurosci 1:39–60.
Poirazi P, Brannon T, Mel BW. 2003. Pyramidal neuron as two-layer neural network. Neuron 37:989–999.
Rall W. 1959. Branching dendritic trees and motoneuron membrane resistivity. Exp Neurol 1:491–527.
Rall W. 1989. Cable theory for dendritic neurons. In: Koch C, Segev I, editors. Methods in neuronal modeling. Cambridge, MA: The MIT Press. p 29–38.
Redish AD, Touretzky DS. 1997. Cognitive maps beyond the hippocampus. Hippocampus 7:15–35.
Redish AD, McNaughton BL, Barnes CA. 2000. Place cell firing shows an inertia-like process. Neurocomputing 32–33:235–241.
Reyes A. 2001. Influence of dendritic conductances on the input-output properties of neurons. Annu Rev Neurosci 24:653–675.
Rudolph M, Destexhe A. 2003a. A fast-conducting, stochastic integrative mode for neocortical neurons in vivo. J Neurosci 23:2466–2476.
Rudolph M, Destexhe A. 2003b. Tuning neocortical pyramidal neurons between integrators and coincidence detectors. J Comput Neurosci 14:239–251.
Samsonovich A, McNaughton BL. 1997. Path integration and cognitive mapping in a continuous attractor neural network model. J Neurosci 17:5900–5920.
Sarnthein J, Petsche H, Rappelsberger P, Shaw GL, von Stein A. 1998. Synchronization between prefrontal and posterior association cortex during human working memory. Proc Natl Acad Sci USA 95:7092–7096.
Sauseng P, Klimesch W, Doppelmayr M, Hanslmayr S, Schabus M, Gruber WR. 2004. Theta coupling in the human electroencephalogram during a working memory task. Neurosci Lett 354:123–126.
Seidenbecher T, Laxmi TR, Stork O, Pape HC. 2003. Amygdalar and hippocampal theta rhythm synchronization during fear memory retrieval. Science 301:846–850.
Seung HS. 1996. How the brain keeps the eyes still. Proc Natl Acad Sci USA 93:13339–13344.
Sharp PE. 1997. Subicular cells generate similar spatial firing patterns in two geometrically and visually distinctive environments: comparison with hippocampal place cells. Behav Brain Res 85:71–92.
Skaggs WE, McNaughton BL, Wilson MA, Barnes CA. 1996. Theta phase precession in hippocampal neuronal populations and the compression of temporal sequences. Hippocampus 6: 149–172.
Soltész I, Deschenes M. 1993. Low and high-frequency membrane potential oscillations during theta activity in CA1 and CA3 pyramidal neurons of the rat hippocampus under ketamine-xylazine anesthesia. J Neurophysiol 70:97–116.
Spencer WA, Kandel ER. 1961. Electrophysiology of hippocampal neurons. IV. Fast prepotentials. J Neurophysiol 24:272–285.
Stam CJ, van Cappellen van Walsum AM, Micheloyannis S. 2002. Variability of EEG synchronization during a working memory task in healthy subjects. Int J Psychophysiol 46:53–66.
Tesche CD, Karhu J. 2000. Theta oscillations index human hippocampal activation during a working memory task. Proc Natl Acad Sci USA 97:919–924.
Tsodyks MV, Skaggs WE, Sejnowski TJ, McNaughton BL. 1996. Population dynamics and theta phase precession of hippocampal place cell firing: a spiking neuron model. Hippocampus 6:271–280.
Vanderwolf CH. 1969. Hippocampal electrical activity and voluntary movement in the rat. Electroencephalogr Clin Neurophysiol 26:407–418.
Vetter P, Roth A, Hausser M. 2001. Propagation of action potentials in dendrites depends on dendritic morphology. J Neurophysiol 85:926–937.
Wallenstein GV, Hasselmo ME. 1997. GABAergic modulation of hippocampal activity: sequence learning, place field development, and the phase precession effect. J Neurophysiol 78:393–408.
Williams SR. 2004. Spatial compartmentalization and functional impact of conductance in pyramidal neurons. Nat Neurosci 7:961–967.
Williams SR, Stuart GJ. 2003. Role of dendritic synapse location in the control of action potential output. Trends Neurosci 26:146–154.
Winson J. 1978. Loss of hippocampal theta rhythm results in spatial memory deficit in the rat. Science 201:160–163.
Wong RK, Prince DA, Basbaum AI. 1979. Intradendritic recordings from hippocampal neurons. Proc Natl Acad Sci USA 76:986–990.
Yamaguchi Y. 2003. A theory of hippocampal memory based on theta phase precession. Biol Cybern 89:1–9.
Yamaguchi Y, Aota Y, McNaughton BL, Lipa P. 2002. Bimodality of theta phase precession in hippocampal place cells in freely running rats. J Neurophysiol 87:2639–2642.
Ylinen A, Soltész I, Bragin A, Penttonen M, Sík A, Buzsáki G. 1995. Intracellular correlates of hippocampal theta rhythm in identified pyramidal cells, granule cells, and basket cells. Hippocampus 5:78–90.
Zugaro MB, Monconduit L, Buzsáki G. 2005. Spike phase precession persists after transient intrahippocampal perturbation. Nat Neurosci 8:67–71.

APPENDIX

The membrane potential of the conducance-based two-compartmental model was described by Hodgkin–Huxley formal-

ism. Somatic and dendritic membrane potentials obeyed standard current balance equations:

$$C_{\mathrm{m}}\dot{V}_{\mathrm{s}}(t) = -I_{\mathrm{Ls}}(t) - I_{\mathrm{Na}}(t) - I_{\mathrm{K-DR}}(t) + I_{\mathrm{As}}(t) + I_{\mathrm{s}}(t)$$
$$C_{\mathrm{m}}\dot{V}_{\mathrm{d}}(t) = -I_{\mathrm{Ld}}(t) - I_{\mathrm{Ca}}(t) - I_{\mathrm{K-C}}(t) + I_{\mathrm{Ad}}(t) + I_{\mathrm{d}}(t)$$

Leak currents were

$$I_{\mathrm{Ls}}(t) = g_{\mathrm{L}}[V_{\mathrm{s}}(t) - V_{\mathrm{L}}]$$
$$I_{\mathrm{Ld}}(t) = g_{\mathrm{L}}[V_{\mathrm{d}}(t) - V_{\mathrm{L}}]$$

Axial currents were

$$I_{\mathrm{As}}(t) = g_{\mathrm{c}}/p[V_{\mathrm{d}}(t) - V_{\mathrm{s}}(t)]$$
$$I_{\mathrm{Ad}}(t) = g_{\mathrm{c}}/(1-p)[V_{\mathrm{s}}(t) - V_{\mathrm{d}}(t)]$$

Voltage-dependent currents were the fast Na^+ current, the delayed rectifier K^+ current, the noninactivating Ca^{2+} current, and the Ca^{2+}-dependent K^+ current

$$I_{\mathrm{Na}}(t) = g_{\mathrm{c}}/(1-p)[V_{\mathrm{s}}(t) - V_{\mathrm{Na}}]$$
$$I_{\mathrm{K-DR}}(t) = g_{\mathrm{K-DR}}n^4(t)[V_{\mathrm{s}}(t) - V_{\mathrm{K}}]$$
$$I_{\mathrm{Ca}}(t) = g_{\mathrm{Ca}}s^4(t)[V_{\mathrm{d}}(t) - V_{\mathrm{Ca}}]$$
$$I_{\mathrm{K-C}}(t) = g_{\mathrm{K-C}}c(t)\chi(t)[V_{\mathrm{d}}(t) - V_{\mathrm{K}}],$$

where $\chi(t) = \min[\mathrm{Ca}(t)/750, 1]$ and $\dot{\mathrm{Ca}}(t) = -0.13\ I_{\mathrm{Ca}}(t) - 0.075\ \mathrm{Ca}(t)$. Gating variables *m, h, n, s,* and *c* obeyed first order kinetics: for any *x* gating variable $\dot{x}(t) = \alpha_x[V(t)]\ [1 - x(t)] - \beta_x[V(t)]\ x(t)$; however, *m* was approximated with its steady-state value $m_\infty(t) = \alpha_m[V(t)]/\{\alpha_m[V(t)] + \beta_m[V(t)]\}$. Rate variables were

$$\alpha_m[V_{\mathrm{s}}(t)] = 0.32[-46.9 - V_{\mathrm{s}}(t)]/(\exp\{[-46.9 - V_{\mathrm{s}}(t)]/4\} - 1)$$
$$\beta_m[V_{\mathrm{s}}(t)] = 0.28[V_{\mathrm{s}}(t) + 19.9]/(\exp\{[V_{\mathrm{s}}(t) + 19.9]/5\} - 1)$$
$$\alpha_h[V_{\mathrm{s}}(t)] = 0.128\exp\{[-43 - V_{\mathrm{s}}(t)]/18\}$$
$$\beta_h[V_{\mathrm{s}}(t)] = 4/(1 + \exp\{[-20 - V_{\mathrm{s}}(t)]/5\})$$
$$\alpha_n[V_{\mathrm{s}}(t)] = 0.016[-24.9 - V_{\mathrm{s}}(t)]/(\exp\{[-24.9 - V_{\mathrm{s}}(t)]/5\} - 1)$$
$$\beta_n[V_{\mathrm{s}}(t)] = 0.25\exp\{0.5 - 0.025[V_{\mathrm{s}}(t) + 60]\}$$
$$\alpha_s[V_{\mathrm{d}}(t)] = 1.6/(1 + exp\{-0.072[V_d(t) - 5]\})$$
$$\beta_s[V_{\mathrm{d}}(t)] = 0.02[V_d(t) + 8.9]/(\exp\{[V_d(t) + 8.9]/5\} - 1)$$
$$\alpha_c[V_{\mathrm{d}}t] = \exp\{[V_d(t) + 50]/11 - [V_d(t) + 53.5]/27\}/18.975 \cdot \mathcal{H}[-V_{\mathrm{d}}(t) - 10] + 2\exp\{[-V_d(t) - 53.5]/27\} \cdot \mathcal{H}[V_d(t) + 10]$$
$$\beta_c[V_{\mathrm{d}}(t)] = (2\exp\{[-V_d(t) - 53.5]/27\} - \alpha_c[V_d(t)]) \cdot \mathcal{H}[-V_d(t) - 10],$$

where $\mathcal{H}$ is the Heaviside function.

Passive parameters of the model were $C_{\mathrm{m}} = 1\ \mu\mathrm{F/cm^2}$, membrane capacitance; $g_{\mathrm{L}} = 0.3\ \mathrm{mS/cm^2}$, leak conductance (except in Fig. 2A2); $V_{\mathrm{L}} = -60\ \mu\mathrm{V}$, leak reversal potential; $g_{\mathrm{c}} = 0.005\ \mathrm{mS/cm^2}$, axial conductance between the soma and the dendrite; and $P = 0.1$, soma/cell surface area ratio. Equilibrium potentials (in mV) and maximal channel conductances (in $\mathrm{mS/cm^2}$) of active conductances were $V_{\mathrm{Na}} = 60$, $V_{\mathrm{K}} = -75$, $V_{\mathrm{Ca}} = 80$ and $g_{\mathrm{Na}} = 30$, $g_{\mathrm{K\text{-}DR}} = 15$, $g_{\mathrm{Ca}} = 10$, $g_{\mathrm{K\text{-}C}} = 15$.